Unsteady Flow Physics and Performance of a One-and-1/2-Stage Unshrouded High Work Turbine

T. Behr
Turbomachinery Laboratory,
Swiss Federal Institute of Technology,
8092 Zurich, Switzerland
e-mail: behr@lsm.iet.mavt.ethz.ch

A. I. Kalfas
Deparment of Mechanical Engineering,
Aristotle University of Thessaloniki,
Greece

R. S. Abhari
Turbomachinery Laboratory,
Swiss Federal Institute of Technology,
8092 Zurich, Switzerland

This paper presents an experimental study of the flow mechanisms of tip leakage across a blade of an unshrouded turbine rotor. It shows the design of a new one-and-1/2-stage, unshrouded turbine configuration, which has been developed within the Turbomachinery Laboratory of ETH Zurich. This test case is a model of a high work ($\Delta h/u^2=2.36$) *axial turbine. The experimental investigation comprises data from unsteady and steady probe measurements, which has been acquired around all the bladerows of the one-and-1/2-stage, unshrouded turbine. A newly developed 2-sensor Fast Response Aerodynamic Probe (FRAP) technique has been used in the current measurement campaign. The paper contains a detailed analysis of the unsteady interaction between rotor and stator blade rows, with particular attention paid on the flow in the blade tip region. It has been found that the interaction of the rotor and the downstream stator has an influence on the development of the tip leakage vortex of the rotor. The vortex is modulated by the stator profiles and shows variation in size and relative position to the rotor trailing edge when it stretches around the stator leading edge. Thereby a deflection of the tip leakage vortex has been observed, which expresses in a varying circumferential distance between two neighboring vortices of* ±20% *of a rotor pitch. Furthermore, a significant influence of quasi-stationary secondary flow features of the upstream stator row on the secondary flow of the rotor has been detected. The geometry and flow field data of the one-and-1/2-stage turbine will be available to the turbomachinery community for validation and improvement of numerical tools.* [DOI: 10.1115/1.2447707]

Introduction

Modern gas turbine designs aim to reach highest possible turbine entry temperatures in order to increase cycle efficiency and turbine specific work. Due to the limitation of the material, rotating blade rows of high-pressure gas turbine stages are designed as unshrouded rotors to reduce mechanical stress. In addition, different cooling strategies have been developed in order to achieve adequate life for all parts that are exposed to these high-temperature gas flows. One critical region for cooling in a high-pressure turbine that remains is the blade tip area. Due to its function of sealing the rotating blade against the stationary casing flow path, this region experiences high thermal loads and is typically difficult to cool. Another way of increasing turbine cycle efficiency is the reduction of aerodynamic losses. The unshrouded design of high-pressure rotor blade rows introduces high losses due to tip leakage flows. Booth et al. [1] found them to be in the order of up to one third of the overall stage losses.

Several strategies for reducing losses due to blade tip gap flows have been subject to a number of investigations in the past decades. According to Denton [2] the loss related to over tip flows is proportional to a discharge coefficient. Further it scales with the velocity distribution around the blade tip, and thus with the loading of the blade tip.

One way of changing the discharge coefficient without effecting significantly the pressure distribution around the tip profile is through modifying the blade tip geometry. Contouring can be done by including squealer rims or radii on the edges of the tip. Booth [3] presented test series of different tip geometries and evaluated the related discharge coefficients. Bindon and Morphis [4] tested three different tip geometries in a linear cascade. They found the discharge coefficient is not necessarily representative for the overall loss created due to tip leakage flow. It does not account for losses due to mixing of the tip leakage flow downstream of the rotor. In an investigation of Kaiser and Bindon [5] in a 1.5-stage rotating rig the plain tip has shown the best performance compared to other geometries tested. With a tip containing a radius on the pressure side edge, the vena contracta that usually forms inside the tip gap could be almost completely eliminated. Other studies on rotating rigs concerning this area of research have been presented by Yoshino et al. [6] and Camci et al. [7]. A numerical analysis on the influence of improved tip concepts has been by Chander et al. [8].

The possibility of reducing tip leakage flows due to reduced loading of the tip region has been discussed in De Cecco et al. [9] and Yamamoto et al. [10]. Staubach et al. [11] realized the off-loading of the tip by applying three-dimensional (3D) design strategies to the profiles. Tip lean was found to be beneficial for this purpose, however its application is limited due to stresses within the rotor blade.

Offenburg et al. [12] investigated in the effect of different trenches within the casing around the rotor on efficiency of the stage. The function of trenches within the casing was found to depend on the tip gap height. Until a relative tip gap of 2.3% blade span the straight casing contour has shown the best results.

On the effect of tip leakage in a multi-stage environment, Harvey [13] concluded that no benefit can be gained out of the tip leakage flow once it has formed into a vortex. In order to limit the losses this vortex imposes on subsequent blade rows, the over tip leakage has to be reduced, and thus the strength of the vortex.

Contributed by the International Gas Turbine Institute of ASME for publication in the JOURNAL OF TURBOMACHINERY. Manuscript received June 7, 2006; final manuscript received June 8, 2006. Review conducted by David Wisler. Paper presented at the ASME, Turbo Expo 2006: Land, Sea and Air (GT2006), Barcelona, Spain, May 8–11, 2006. Paper No. GT2006-90959.

Another approach in order to reduce the losses due to tip leakage has been undertaken by Dey et al. [14] and Rao et al. [15,16]. Coolant has been injected from the blade tip into the tip gap in order to reduce the mixing losses due to the tip leakage. Jets at different discrete positions and blowing ratios have been evaluated. An influence of the injection rate on the radial position of the tip leakage vortex and of the injection position on its strength could be detected.

The design of the new test case focuses on the set research objectives and orientates on findings of previous investigation described above. A 1 1/2 stage turbine configuration, comprising a flat blade tip geometry and a straight rotor casing contour, has been implemented into a continuously operating test rig. Unsteady probe measurement techniques can be applied to measure the complete flow field around the blade rows. The existence of a second stator as well allows the evaluation of tip leakage effects on the performance of subsequent blade rows. The experimental investigation of the new test configuration creates the background for an upcoming study of tip leakage flow phenomena.

Experimental Method

The new research project required some substantial modification to the existing turbine rig of the turbomachinery laboratory. The previous two-stage, shrouded turbine configuration has been successfully used for a number of multi-stage, low-speed investigations, (i.e., Schlienger [17], Pfau [18], Porreca et al. [19], and Behr et al. [20]). A redesign of the entire turbine section made it possible to achieve more realistic flow conditions for the upcoming investigation and, at the same time, it increases the capabilities for measurement access. In the following sub section the new turbine rig will be introduced in more detail.

Research Turbine Facility.

Global System Design. The air loop of the facility is of a quasi-closed type and includes a radial compressor, a two-stage water to air heat exchanger, and a calibrated venturi nozzle for mass flow measurements. Before the flow enters the turbine section, it passes through a 3 m long straight duct, which contains flow straighteners to ensure an evenly distributed inlet flow field. Downstream of the turbine the air loop is open to atmospheric conditions. A dc generator absorbs the turbine power and controls the rotational speed of the turbine. A torque meter measures the torque that is transmitted by the rotor shaft to the generator. The turbine entry temperature (TET) is controlled to an accuracy of 0.3% and the rpm is kept constant within $\pm 0.5\ \text{min}^{-1}$ by the dc generator. The pressure drop across the turbine is stable within 0.3% for a typical measurement day. More information on the test rig can be found in Sell et al. [21].

For the current investigation the test rig turbine section has been redesigned to meet the following objectives:

1. Model of unshrouded, high-pressure gas turbine stage:
   - High-pressure gas turbine blade design;
   - High stage loading;
   - Compressibility effects;
   - Low aspect ratio; and
   - Realistic rotor exit flow field through second stator.
2. High accessibility for flow measurements:
   - Probe access to inlet and exit of each blade row; and
   - Optical access to all blade rows.
3. Flexibility for different research projects:
   - Modular design for fast hardware changes;
   - Universal measurement windows; and
   - Clocking of stator blade rows.

Table 1 Main parameter of "LISA" 1.5-stages axial turbine research facility at design operating point

Turbine	CFD	Exp.
Rotor speed (rpm)	2700	2700
Pressure ratio (1.5-stage, total to static)	1.58	1.60
Turbine entry temperature (°C)	55	55
Total inlet pressure (bar abs norm)	1.4	1.4
Mass flow (kg/s)	12.15	12.13
Shaft power (kW)	289	292[a]
Hub/tip diameter (mm)	660/800	660/800
First stage	CFD	Exp.
Pressure ratio (first stage, total to total)	1.35	1.35
Degree of reaction (-)	0.39	0.39
Loading coefficient $\psi=\Delta h/u^2$ (-)	2.21	2.36[b]
Flow coefficient $\phi=c_x/u$ (-)	0.63	0.65

[a]From torquemeter.
[b]From five-hole-probe measurement.

Given the fact that the compressor pressure ratio is limited to $\Pi_{c,\max}=1.5$, the new turbine contains only one highly loaded rotating blade row. This design was chosen in order to maximize flow Mach numbers and the loading coefficient of the turbine stage. The static pressure of the flow at exit of the first stage reaches almost the level of the atmospheric pressure, before it is further reduced by the second stator. The existence of a second stator has been set as a design intention in order to have the potential field of a subsequent stage. Since the turbine rig is open to atmosphere at the exit, a tandem de-swirl vane arrangement recovers the static pressure at exit of the second stator back to the ambient level. This design increases the available pressure ratio at the first stage to the maximum possible. The key parameters of the new turbine configuration are presented in Table 1 as a comparison between computational fluid dynamics (CFD) prediction and experimental validation.

Mechanical Design

A cross-section cut of the turbine section is shown in Fig. 1, as well as an expanded view of the test section in Fig. 2. The turbine mechanical design allows quick and precise assembly of all parts, which ensures a high level of repeatability and comparability between different builds.

First stator and rotor are manufactured as bladed disks (blisks) out of one piece (see Fig. 3). The manufacturing process ensures an accuracy of the profile shape of ±0.05 mm with respect to the design intention. The roughness of the profiles and flow channels are hand polished down to $Ra=0.8\ \mu$m. The second stator ring is divided into several segments, which gives the opportunity of individual instrumentation of single stator profiles.

The first stator row is fixed to a support ring that can be continuously positioned in circumferential direction. This feature opens the possibility to clock the two stator blade rows relatively to each other.

Measurement access for intrusive and nonintrusive techniques is provided around all blade rows. Aerodynamic probes can be automatically positioned inside the flow by a four-axis numerically controlled traversing system with high accuracy in every direction. In order to minimize the disturbance of the flow due to the probe access, only small holes are placed in the casing rings, which allow a probe to pass through. For the circumferential positioning, the casing ring is then traversed together with the probe.

Inside of the rotor casing ring a multi-purpose window has been implemented which covers around five rotor pitches. It can be traversed as well in a circumferential direction. Through that access it is possible to apply optical techniques, such as particle in velocity (PIV).

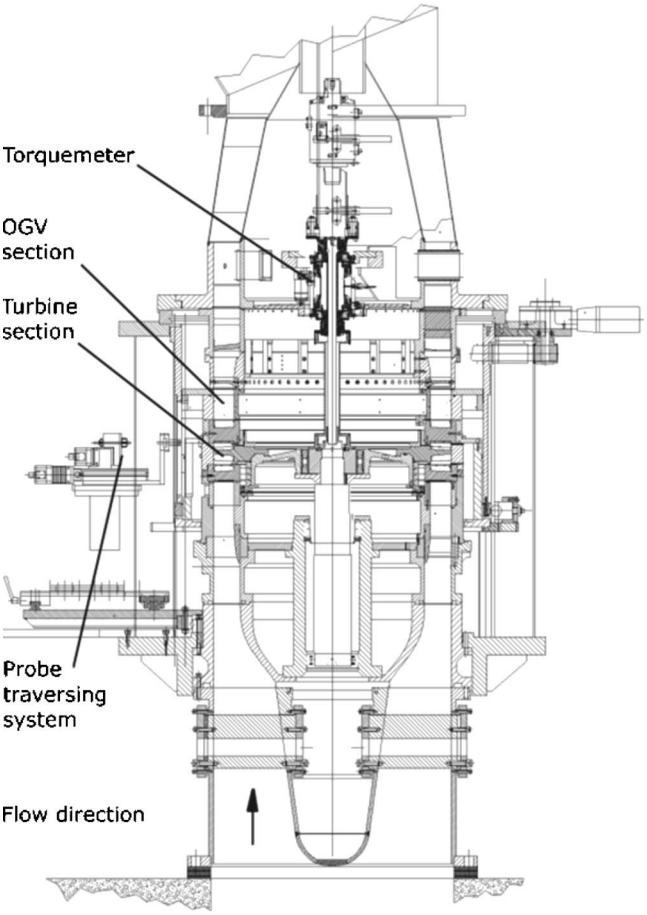

Fig. 1 "LISA" 1 1/2 stage axial turbine facility

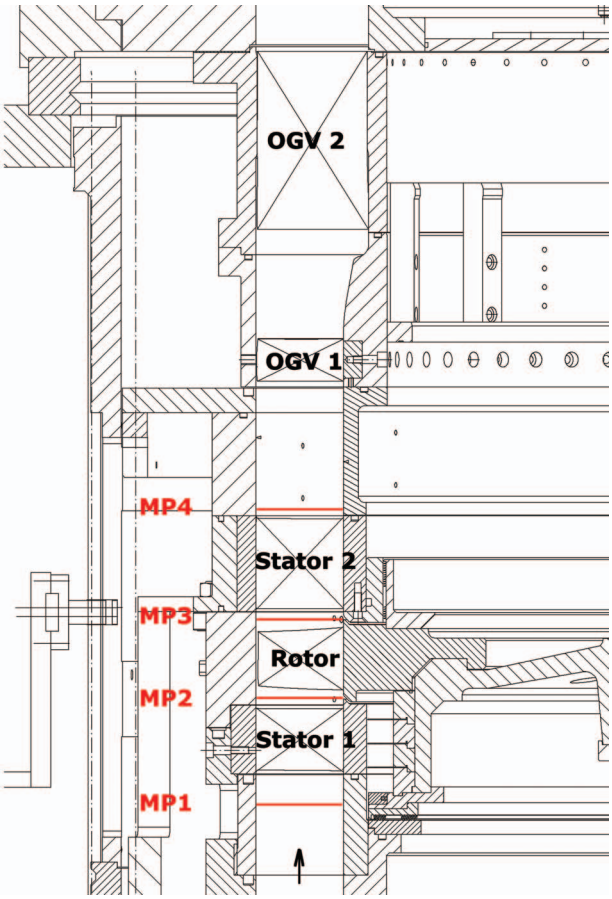

Fig. 2 1.5-stage turbine section with probe measurement planes and tandem exit guide vane section

Bladerow Design

All bladerows of the new 1 1/2 stage, unshrouded turbine have been designed at the Turbomachinery Laboratory. The geometry data are available to the public domain from Behr et al. [22]. A number of commercial and in-house design and validation tools have been combined to establish a development algorithm, which lead to the final design of four new turbine blade rows:

1. *1D design*: The meanline design of the new turbine has been done using an in-house tool of the Turbomachinery Laboratory of ETH Zurich (LSM). In addition the commercial tool Concepts NREC Axial has been applied.
2. *Profile generation*: The commercial tool Concepts NREC Axcad has been used for creating the baseline 2D profiles at different span positions and to define the stacking line of the 3D profiles. The implemented profile generator is based on an 11-parameter, axial turbine airfoil geometry model of Pritchard [23].
3. *Profile optimization*: The baseline 2D blade profiles have been optimized by running the industrial CFD code Stage3D in an inverse design mode. By defining the loading distribution of a 2D profile, the code corrects the geometry of the profile until it matches to the given distribution. The method has been developed and introduced by Troxler [24]. As a result of this optimization Fig. 4 shows the profile of the rotor at span positions hub, midspan and tip and its corresponding distributions of relative isentropic surface Mach number (Fig. 5).
4. *Aerodynamic design validation*: The industrial CFD code Stage3D has been used to validate the performance of the 3D blade geometries. All profiles have been modeled using grids created out of straight *H* meshes. Calculations were performed on single rows as well as in the multi-stage domain. The 3D steady and unsteady Navier–Stokes multistage solver Stage3D has been derived from the original Dawes code BTOB3D [25], running a discretization scheme from Jameson and Baker [26]. The one-equation turbulence models of Spalart and Allmaras [27] has been chosen in the current case. When running steady state the solver uses a so-called mixing-plane between rotating and nonrotating cascades, which mixes out circumferential variations. The averaging for the mixing planes is done, using a consistent

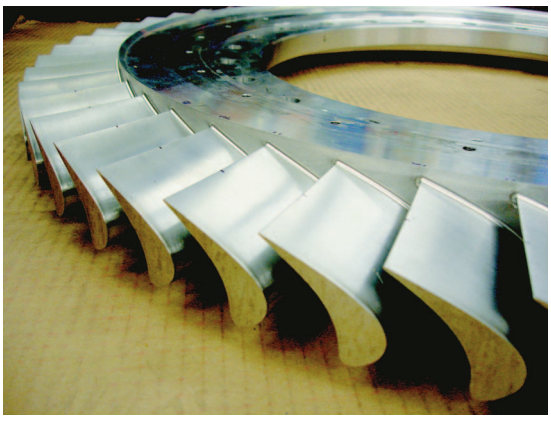

Fig. 3 Rotor blisk of the 1.5-stage unshrouded turbine

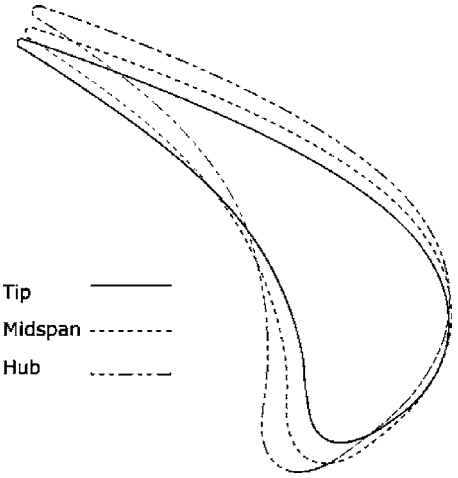

Fig. 4 Profile geometry of rotor blade at three span positions

approach from Denton [2]. The code has been further validated and improved by Mokulys et al. [28].

5. *Computer aided design (CAD) design*: The construction of 3D CAD models for manufacturing has been done using CATIA V5. It uses a cubic spline interpolation to connect the imported 2D profiles to a 3D model. Splines inbetween the profiles can be defined to prevent undesirable twisting of the 3D geometry. Important design geometry parameters, such as trailing edge radii, or throat areas, can be checked very accurately with this tool.
6. *Finite element method (FEM) validation*: To check the structural integrity of the rotor the FEM tool Abaqus has been applied.

The flow is turned by the first stator blade row to an average exit angle of about 73 deg. Thereby it reaches an average Mach numbers of $Ma_{av}=0.54$ at the exit of the first stator. The profiles of the both stators follow a constant exit angle design. Within the rotor the flow is redirected by an average turning angle of $\varepsilon=122$ deg, which results in a mean loading coefficient of $\psi=2.36$. The radial tip gap between rotor and casing has been selected to be of 1% of the blade span. The flow enters the second stator blade row at an average absolute flow angle of $\phi_{av}=-42$ deg and leaves it again at $\phi_{av}=64$ deg. It is thereby accelerated to an average exit Mach number of $Ma_{av}=0.48$. A more detailed list of profile parameters can be found in Table 2.

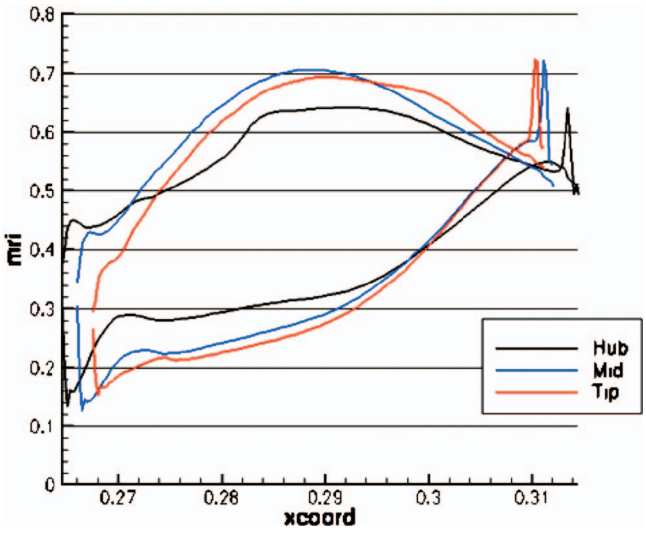

Fig. 5 Distribution of relative isentropic Mach numbers on the rotor at three span positions

Table 2 Characteristic geometry and performance parameters of the 1.5-stage turbine configuration (performance values derived from five-hole-probe measurements at design operating point)

	Stator 1	Rotor	Stator 2
Number of blades	36	54	36
Inlet flow angle (deg) (midspan)	0	54	−42
Exit flow angle (deg) (midspan)	73	−67	64
Solidity (chord/pitch)	1.27	1.41	1.34
Mean stagger angle (deg)	52.8	39.4	34.5
Aspect ratio (span/chord)	0.87	1.17	0.82
Zweifel number (-)	0.7	1.0	1.0
Profile stacking	LE	CoG	LE
Blade row relative exit Mach numbers (-) (average)	0.54	0.50	0.48
Reynolds number based on true chord and blade row relative exit velocity (-)	$7.1\cdot10^5$	$3.8\cdot10^5$	$5.1\cdot10^5$

During the design process it was decided to use a tandem outlet guide vane ensemble. The first outlet guide vane (OGV) row was designed to be adjustable in a range of stagger angle of ±10 deg. The second OGV row is fixed and turns the flow back to a 0 deg exit flow angle. Since the turbine exit is open to atmosphere, this design gives the possibility to throttle the exit of the turbine and hence to adjust the pressure ratio of the 1.5-stage turbine stages.

The first OGV has been design using the NACA profile definition of the Concepts AXCAD profile generator (see Fig. 6). The intended turning of this profile is in the order of 18 deg. In order to prevent flow separation at the endwalls and related unsteady flow instabilities, hub and tip lean have been applied for the profile stacking. At the hub a lean angle of 30 deg has been applied

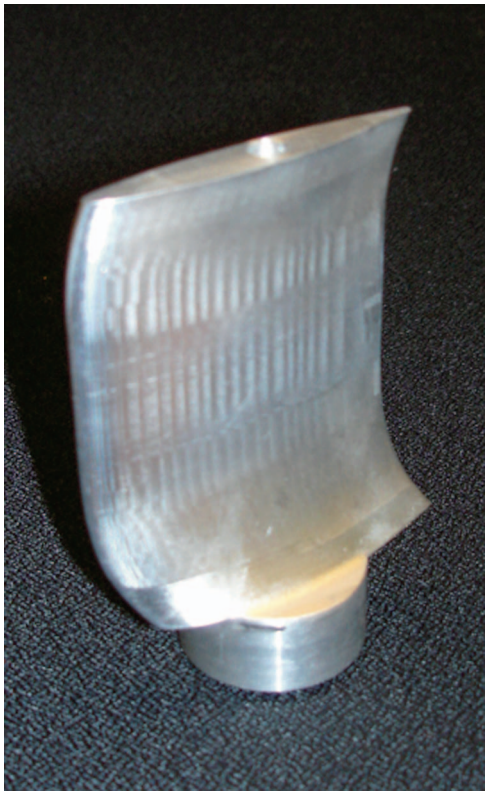

Fig. 6 Profile of first outlet guide vane row

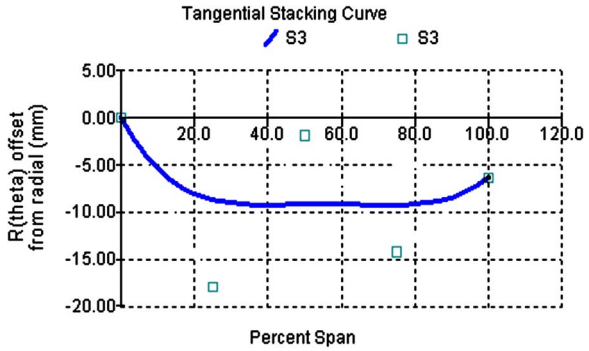

Fig. 7 Stacking definition of first OGV row

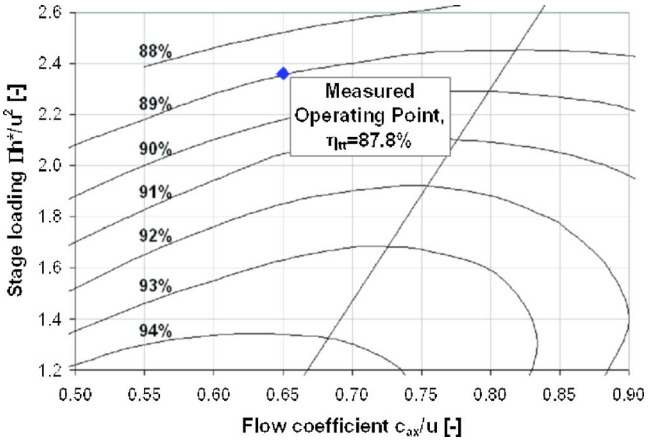

Fig. 8 Smith chart with measured operating point and determined total-to-total efficiency (reproduced after Ref. [32])

from 0% to 25% span. At the tip a lean angle of 15 deg has been applied from 90% to 100% span. The stacking definition is presented in Fig. 7.

The second OGV row comprises of a cylindrical profile which turns the flow from 46 deg to 0 deg. This extreme turning can be realized by the special shape of the profile, which accelerates the flow almost until the trailing edge, where a step diffuser releases it into the duct. With this design no separation and hence no blockage occurs (see Table 3).

Measurement Technology. The experimental flow field data presented in the paper originate from time-resolved probe measurement in planes downstream of each bladerow. The unsteady pressure measurement technology of the fast response aerodynamic probes (FRAP) has been developed at the LSM [29,30]. The mainstream flow field was measured using a novel 1.8 mm tip diameter, two-sensor FRAP probe in virtual-four-sensor mode providing 2D, time-resolved flow field information. Each measurement plane is resolved by a grid of 39 points in radial direction which are clustered close to the endwalls and 20 equally spaced points in circumferential direction, covering one stator pitch. The time-resolved pressures signal is acquired at each measurement point at a sampling rate of 200 kHz over a time of 2 s. The data sets are processed to derive basic flow quantities, i.e., total and static pressure, flow yaw and pitch angles, velocity components, and Mach number by applying a phase lock average over 85 rotor revolutions. For the data evaluation three consecutive rotor passages were selected. Each rotor passage is resolved in time by 82 samples. The frequency response of the probe allows capturing flow features at frequencies up to 35 kHz. With this new two-sensor probe technology it is possible to provide also flow turbulence information [31]. The FRAP probe technology provides also temperature data at a frequency of up to 10 Hz.

Results and Discussion

In the following section the analysis of the measured performance and flow field data will be presented. Particular attention will be paid on flow effects, which will influence the evolution of rotor tip leakage secondary flows.

Table 3 Characteristic geometry of the tandem outlet guide vane ensemble

	OGV 1	OGV 2
Number of blades	54	48
Inlet flow angle (deg) (midspan)	64[a]	46
Exit flow angle (deg) (midspan)	46[a]	0
Solidity (chord/pitch)	1.4	—
Mean stagger angle (deg)	53	—
Aspect ratio (span/chord)	1.16	—

[a]Adjustable stagger angle.

Performance Evaluation. The instrumentation of the test facility allows the measurement of rig operation parameters, such as torque of the second stage and massflow. This allows the calculation of mechanical efficiency. The integral character of this value does not resolve any spanwise efficiency distribution. It is defined as the ratio of specific shaft power over the enthalpy difference of the isentropic expansion

$$\eta_m = \left(\frac{\omega \cdot M}{\dot{m}}\right) \Big/ \left\{ c_p T_{\text{in}} \left[1 - \left(\frac{p_{t,\text{out}}}{p_{t,\text{in}}} \right)^{(\kappa-1)/\kappa} \right] \right\} \qquad (1)$$

For the new turbine configuration a mechanical total-to-total efficiency value of the first stage of $\eta_{tt}=87.8\%$ has been derived. In order to relate this value to an empirical data basis, the operating point has been plotted in a Smith chart [32] (see Fig. 8). The actual value differs by about 1% from the expectation.

The performance of the tandem outlet guide vane ensemble has been a crucial design issue, since it is defining the pressure ratio and hence the overall performance of the 1.5-stage turbine. In the performance measurements of the final turbine it could be verified that the design of the OGV ensemble reached the intended recovery of static pressure. The comparison of design and experimental values is presented in Fig. 9. It was observed that the first OGV row recovers about 25% more static pressure than expected, which increases the range of possible pressure ratios of the turbine.

Flow Field of the First Stator. The flow field into the first stator has a uniform distribution of total pressure from 20% to

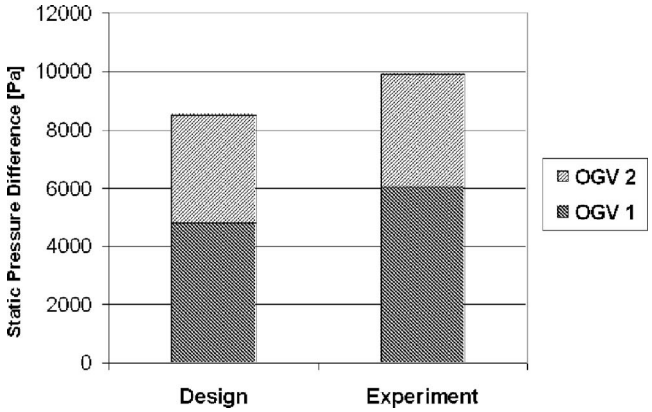

Fig. 9 Comparison of first OGV static pressure recovery between design and experiment

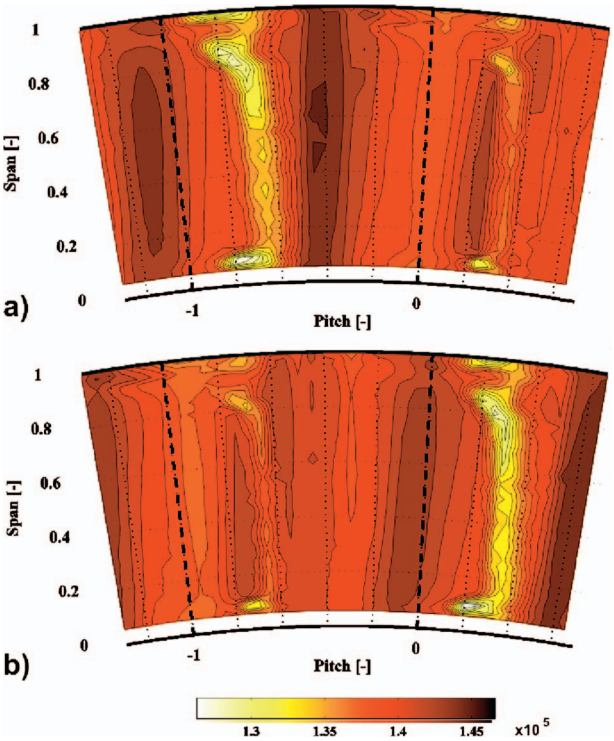

Fig. 10 Distribution of measured total pressure at exit of stator 1 at the time instants of a rotor blade passing period: (*a*) *t*/*T*=0.00; and (*b*) *t*/*T*=0.50

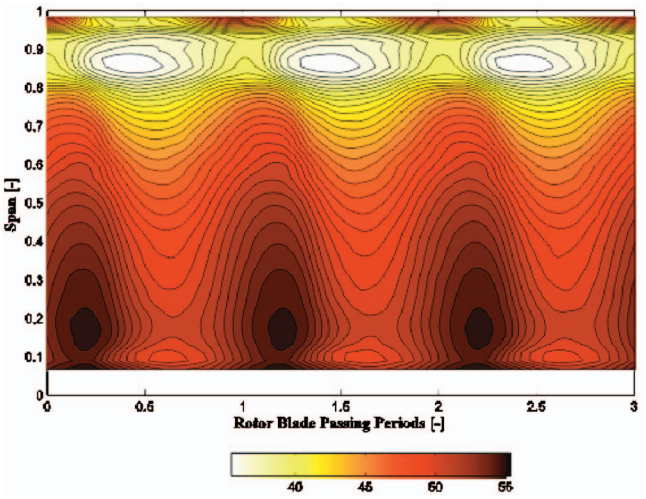

Fig. 11 Circumferentially mass-averaged distribution of measured relative flow yaw angle at exit of stator 1 versus time of three rotor blade passing periods

80% span. A region within 20% span from the endwalls is affected by boundary layers, which result from the inlet section of the turbine. The inlet flow field of the stator is symmetric between the hub and tip region.

In order to evaluate the flow field out of a stationary blade row it is usually sufficient to look at steady information of the flow properties. The general performance of a blade row can be captured well, when plotting time-averaged spanwise distributions of flow angles and pressures. With focus on the development of the rotor tip leakage flow it is important to consider the time-resolved flow field. The variation of the stator exit flow field over time will affect considerably the unsteady flow, especially in the rotor blade tip region.

The interaction between the stator exit flow field and the passing rotor is demonstrated in Fig. 10. On the area of two stator pitches, the distribution of total pressure is plotted for two time instants of one rotor blade passing period. In both figures the secondary flow features that leave the stator blade row can be identified. The core of the stator hub passage vortex reaches from the hub casing wall until 10% span. The stator passage vortex can be found between 80% and 90% span. Both vortices are connected by the stator wake, which shows a straight shape and is almost perfectly aligned in the radial direction. The fact that all main secondary flow features of the first stator are aligned along one circumferential position implies a high potential for improving turbine performance through clocking the stator blade rows. A dependency on the effect of clocking on the relative position of secondary flow features has been found by Behr et al. [20]. At the casing endwall the formation of an additional secondary flow feature can be identified. It originates at the casing endwall within the stator passage after the tip passage vortex has left the suction side and gives space to a formation of new boundary layer. This effect can be reduced by introducing a lean angle to the stacking of the profile in the tip region. In the current case this option has been discarded during the design process to create a baseline case that allows unrestricted probe access to all the stator passage. Generally, the flow field out of the stator shows a clear two-dimensional character over a range from 10% to 70% span. At both time instants, shown in Fig. 10, the secondary flow field of one stator pitch vanishes almost completely due to the vicinity of a rotor leading edge. In the contour plot: (*a*) the wake and both vortices are fully developed and approach the midpitch region of two rotor blades in an undisturbed manner. In this case the total pressure in these areas reaches its minimum value. Due to the 2:3 ratio between stator and rotor blade count, the secondary flow features of the adjoining stator pitch, oppose a static pressure field of a rotor leading edge. Thereby the pressure level rises in these regions such that the total pressure of secondary flow features reaches the level of the undisturbed main flow. Figure 10(*b*) shows the same area after the rotor has moved on by half a rotor pitch. The situation is analog to the one, which has been just described, except for the fact that the phenomena on the two stator pitches are switched.

The pulsation of the flow approaching the rotor blade can be also seen in the circumferentially mass-averaged distribution of relative flow yaw angle at the exit of stator 1. The mass averaging has been done intentionally on the area of one stator pitch, in order to see the local effect of the blade row interaction. In Fig. 11 these spanwise distributions are plotted for three rotor blade passing periods. It was found that in all span positions the rotor relative flow yaw angle varies by ±2.5 deg during the blade passing period. Hereby a linear phase shift between use tip and hub region of around 25% of a rotor blade passing period has been observed. This fact can be seen in the timewise shift of the locations of minimum and maximum flow angles at hub and tip in Fig. 11. The inclination of the contour lines in this plot also indicates the continuous rise toward flow overturning while the rotor leading edge pressure field approaches the wake region of the stator. As soon as it has passed, the flow yaw angles, especially the ones of the secondary flow, reduce quickly as the flow passes along the pressure side of the rotor. The periodic fluctuation of the relative rotor inlet angle also has a direct influence on the power created on a rotor blade. However, the timewise variation of global shaft power is rather low, since the ratio of stator and rotor blade count averages these individual unsteady effects on the rotor blades. Furthermore, Fig. 11 shows the trace of both passage vortices, by a constantly underturned region around 10% and 83% span, as well as an overturning at 93% span. The overturning of the hub passage vortex has not been captured by the probes, due to the vicinity to the wall. The variation of flow yaw angle during one rotor blade passing period, as it has been described on the mass-averaged

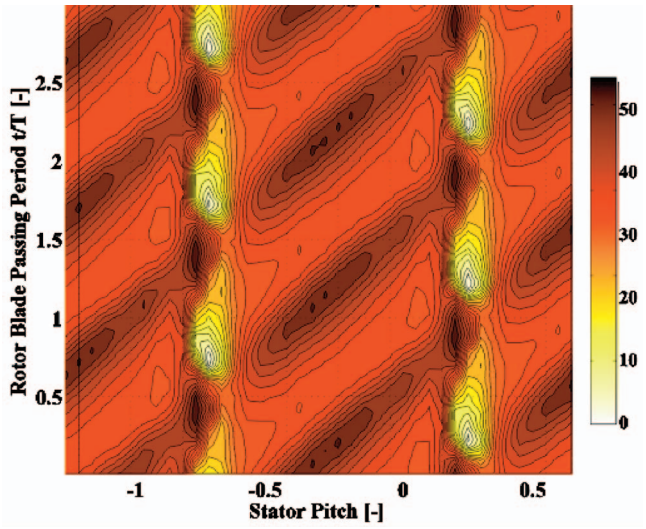

Fig. 12 Circumferential distribution of measured relative flow yaw angle at exit of stator 1 at 83% span versus time of three rotor blade passing periods

spanwise distribution, is much more intense in certain span positions. In the region of the stator tip passage vortex at 83% span, the variation of the relative flow yaw angle reaches locally up to 40 deg. This behavior is illustrated in a time–distance plot at this span position (see Fig. 12). In these kinds of plots, features that are fixed relative to the stationary frame appear as vertical lines. Features traveling with the rotor are visible as inclined parallel structures, which can be assigned to different rotor blades. The reaction of the flow during the interaction of rotor and stator can be seen in the crossing points of those lines.

The timewise variation of the rotor inlet flow angle in span positions near the casing endwall causes incidence on the rotor profile at this position. For this rotor blade profile, the design inlet angle in the tip region is around 40 deg. Due to the blade row interaction, this angle drops here for a short period of time to 0 deg. This variation of the rotor incidence angle will cause an unsteady, fluctuating pressure field around the rotor tip. Hence, the formation of the tip leakage vortex over the blade tip will be influenced according to the pressure variation.

Rotor Exit Flow Field. Within the rotor blade row the radial pressure gradient changes and the general direction of the streamlines is deviated toward the casing. The boundary layers of both hub and tip endwall are creating the passage vortices. At the same time the pressure gradient between pressure and suction side at the blade tip causes the flow in this region to pass through the tip gap. It results in a jet flow across the suction side edge of the blade tip, which mixes again with the main flow and rolls up into a vortex.

In Fig. 13 the time-resolved flow field out of the rotor is presented in the form of a relative total pressure coefficient distribution. All plots are views in the downstream direction on a sector covering two stator pitches. In order to show the variation of the flow field between two rotor blades, four equidistant time steps of one rotor blade passing period are plotted.

Both rotor passage vortices, the tip leakage vortex and the rotor wake, can be clearly identified in all pictures. All of these secondary flow features are traveling with the rotor blades. However, their relative position to the rotor trailing edges, as well as their strength, is not constant. The interaction with the downstream stator row and unsteady flow features originated by the first stator have an effect on their appearance.

The rotor hub and tip passage vortices are located between 18% and 28% blade span, and 65% and 80% blade span, respectively. Both vortices seem to be detached from the suction side of the

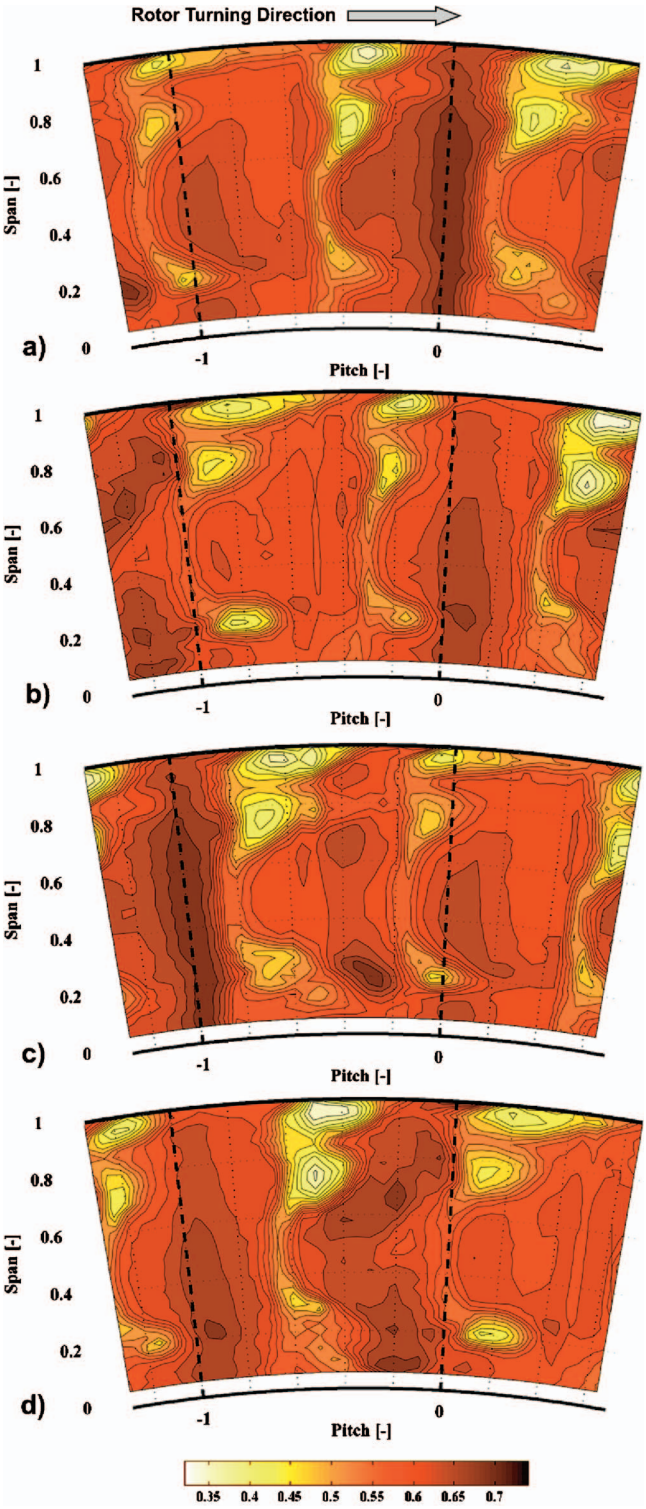

Fig. 13 Distribution of measured relative total pressure coefficient downstream of the rotor at four different rotor blade passing periods: (*a*) *t*/*T*=0.00; (*b*) *t*/*T*=0.25; (*c*) *t*/*T*=0.50; and (*d*) *t*/*T*=0.75

rotor blade, since the cores of these vortices are shifted by up to 20% rotor pitch in a circumferential direction relative to the wake position. This observation can be confirmed by the fact that their shape is almost elliptical, which indicates that there has been no recent restriction from the blade suction side surface. The tip passage vortex shows considerably lower relative total pressures than

the hub passage vortex.

The vicinity of the second stator has an impact on the secondary flow features coming out of the rotor. In Fig. 13 the position of the second stator leading edges is located around the stator pitch positions −1 and 0. In these locations the static pressure field of the second stators is maximal.

At time $t/T=0.00$ both passage vortices at stator pitch position −1.1 are just about to pass a leading edge of the second stator. Therefore in this moment the relative pressure of the passage vortices reaches its maximum value. At the same time the circumferential distance between the cores of the passage vortices and the rotor wake is minimal.

At time $t/T=0.25$ the passage vortices around stator pitch position −0.9 have passed the stator leading edge region and are becoming stronger, as the relative total pressure is reducing. The rotor wake has almost disappeared in this moment due to the influence of the second stator.

At time $t/T=0.50$ both passage vortices around the stator pitch position −0.7 and the corresponding rotor wake can pass unrestricted into the midpitch region of the second stator. At the same time the passage vortices of the preceding rotor blade around stator pitch position −0.1 stretch around the leading edge of the next stator profile. It is the same process as it has been described at $t/T=0.00$ for the other pair of passage vortices. This time shift of $t/T=0.5$ of a rotor blade passing period between the occurrences around two adjoining stator profiles is characteristic of the current 2/3 blade count ratio of stators and rotor.

At time $t/T=0.75$ both passage vortices at stator pitch position −0.5 are still unaffected by the stator leading edges. However, the passage vortex shows a discontinuity since it is leaving its radial position. This behavior will be addressed in the next paragraph. At the left side of the plot in Fig. 13(*d*) a next pair of rotor passage vortices is approaching the stator leading edge at stator pitch position −1.1. With this the loop of one rotor blade passing period is closed.

When observing the relative positions of passage vortices and wake of the rotor, it can be seen that both features show a different reaction to the potential field of the second stator leading edges. The closer the vortices and the wake come to the stator leading edge, the closer they come together. As soon as the vortices have passed the stator leading edge region, the circumferential distance between wake and vortices increases rapidly. Hereby the wake shows a more constant reaction to the potential field of the stator as it does not change the direction of the wake fluid. In contrast to that, the vortices change their flow direction rather quickly from suction to pressure side of the second stator.

Another flow feature has been observed, which is interacting with the hub passage vortex of the rotor. Due to the direction of the rotation of the hub passage vortex, the core of the hub passage vortex lifts up to 22% of the blade span until it reaches the measurement plane. It can be found in this position most of the time. In Fig. 13(*d*) it can be seen that this vortex moves outward up to around 32% span, as another low total pressure area appears close to the hub at −0.5 stator pitch. In the authors' opinion, this low −2 pressure area is a vortical structure which was originated in the first stator, since it always appears periodically at the same location. The hub passage vortex does not merge with this feature but goes around it. The fact that stationary features from the previous stator row can be clearly seen after the rotor indicates a high potential for optimizing stage efficiency by clocking both stator rows.

The behavior of the passage vortices due to the interaction with the second stator leading edge, as it has been described before, applies similarly to the tip leakage vortex. This can be found from the 90% blade span until the casing. The tip leakage vortex can be clearly distinguished from the tip passage vortex, which is located more radially inward at the same circumferential position. Within the rotor passage the tip leakage vortex covers the space around the rotor tip suction side corner. Due to its opposite direction of rotation it displaces the tip passage vortex, as it comes from the pressure side, to a more radially inward position.

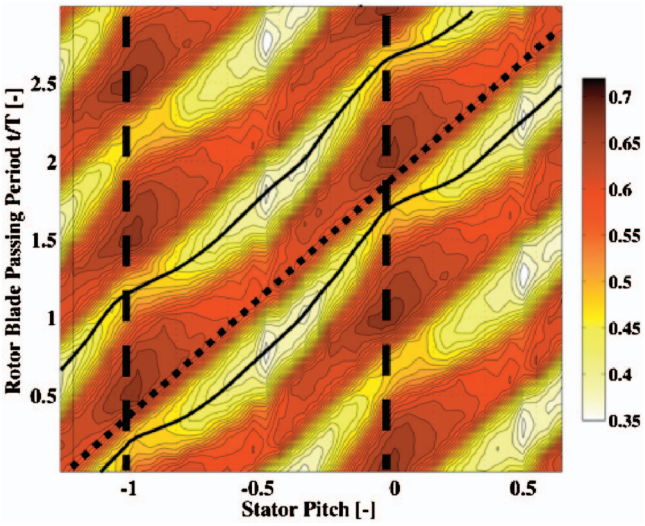

Fig. 14 Circumferential distribution of relative total pressure coefficient versus time at rotor exit at 95% span

The tip leakage vortex also experiences a modulation and deflection due to the second stator pressure field. In order to visualize the changes of the tip leakage vortex, the relative total pressure at the corresponding span position is plotted versus time in Fig. 14. The vertical dashed lines in the figure represent the position of the second stator leading edge. The approximate position of one rotor trailing edge is indicated by the dotted line. Accordingly, the rotor turning direction in the figure is from left to right. The region of the tip leakage vortex can be confined by the high-pressure gradient around it. The extension of the vortex in circumferential direction is minimal when it passes the stator leading edge. In this moment the vortex is being stretched to go around the leading edge of the stator. The stretching of the vortex can be seen in an increased velocity during this time (see Fig. 15). Right afterward the vortex slows down and occupies a larger area. These changes of the vortex size are visualized in Fig. 14. Since the vortex is confined on one side by the suction side surface, the low-pressure

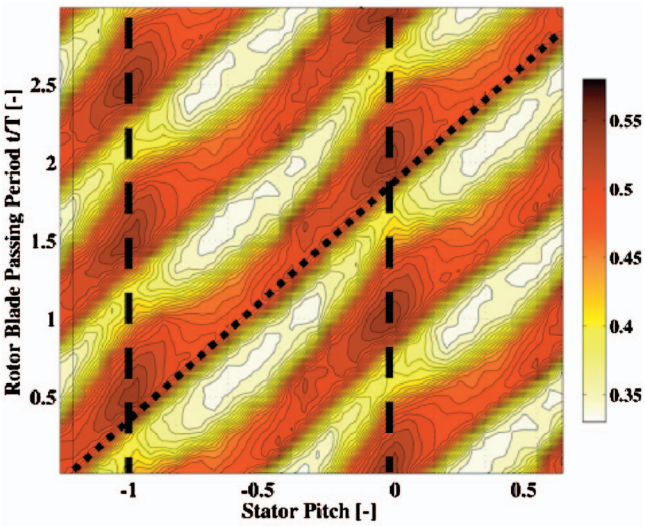

Fig. 15 Circumferential distribution of measured relative mach number versus time at rotor exit at 95% span

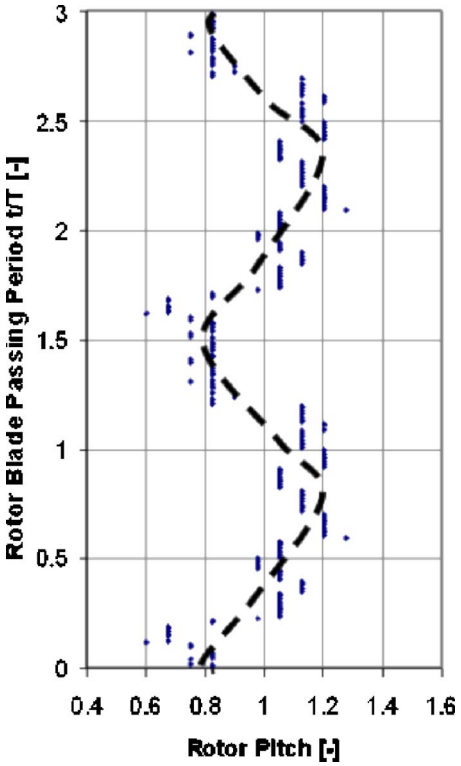

Fig. 16 Circumferential distance between the cores of two adjoining tip leakage vortices plotted versus time

area follows a straight line on its left boundary. The right boundary shows a nonlinear shape, according to the vortex size. The two splines in the figure follow the locations of minimum pressure, which are related to the core of the tip leakage vortex. They show that the residence time of the tip leakage vortex varies between different rotor relative positions. The mechanism of stretching of vortices due to blade row interactions and its relation to loss generation has been addressed in more detail in Chaluvadi et al. [33].

In Fig. 16 the circumferential distance between the two splines of Fig. 14 for each time instant is plotted versus time. These plot shows that the distance between the tip leakage vortices of two neighboring blades is changing by ±20% of a circumferential rotor pitch. This change in distance comes due to the time shifted deflection of the two vortices around the leading edges of the downstream stator.

This alternating deflection of the rotor vortices around the stator leading edge also expresses the instantaneous distribution of relative flow yaw angles at the rotor exit. Figure 17 shows the maximum and minimum deviation of circumferentially mass-averaged relative flow yaw angles from the time mean value. The rotor tip leakage vortex as well as both passage vortices can be clearly identified in the figure considering the considerably higher variation of the flow angle. Hereby the tip leakage vortex and the rotor tip passage vortex change the relative exit angle of the flow by up to ±2.5 deg during one rotor blade passing period. The hub passage vortex achieves ±2.5 deg, whereas the main flow is constant within ±0.7 deg. The change in exit angle contributes in addition to the variation of loading of each rotor blade.

The above mentioned effects show the influence of the pressure field of the downstream stator on the timewise circumferential variation within the rotor relative outlet flow field. An accurate unsteady CFD simulation of the rotor flow field, especially tip leakage secondary flows, should therefore apply to boundary conditions, which describe these circumferential variations, rather than radial profiles only.

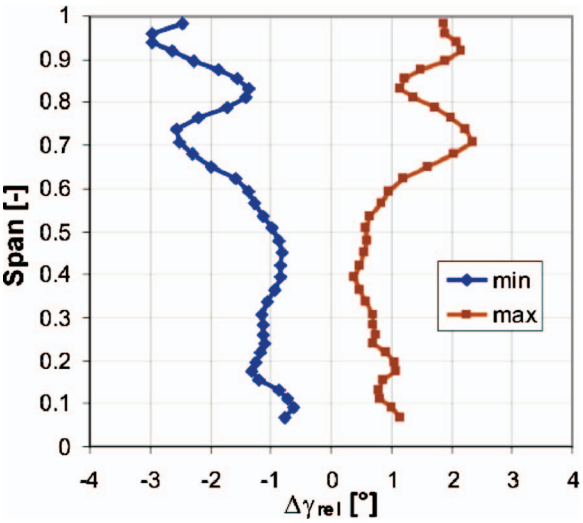

Fig. 17 Maximum and minimum deviation from time-averaged mean value of circumferentially mass-averaged spanwise distribution of relative flow yaw angles at rotor exit

Flow Field Behind Stator 2. The unsteady flow out of the rotor is going to be mixed and accelerated within the passage of the second stator. Any unsteadiness in the exit flow field of the second stator will be due to the flow of the upstream rotor, since no blade row is following downstream. Vortices of the rotor will be stretched around the stator leading edge, whereas remains may appear periodically at the stator exit. An impression of the highly three-dimensional flow field is given in Fig. 18. The distribution of total pressure coefficients is shown for two time instants of a rotor blade passing period. Considering the two neighboring stator

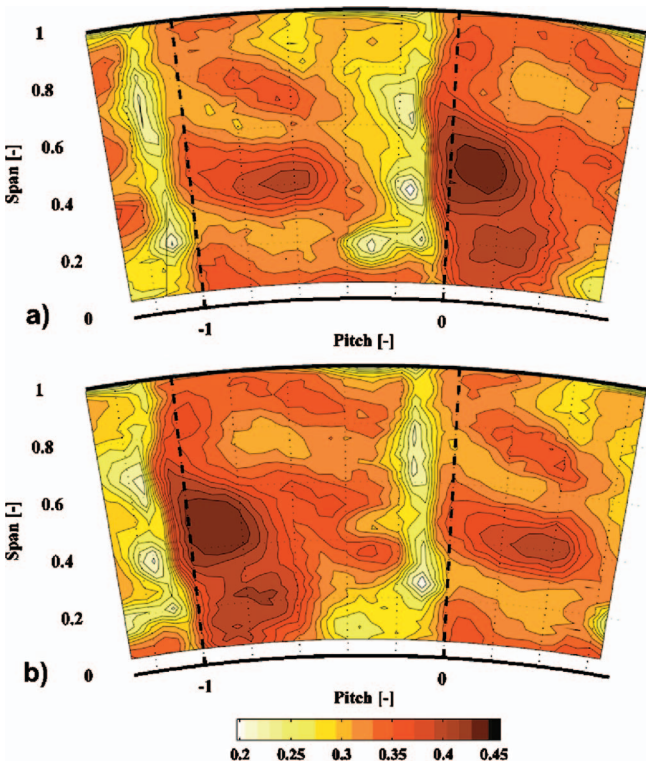

Fig. 18 Distribution of measured total pressure coefficient at the exit of stator 2 at rotor blade passing periods: (*a*) $t/T = 0.00$; and (*b*) $t/T = 0.50$

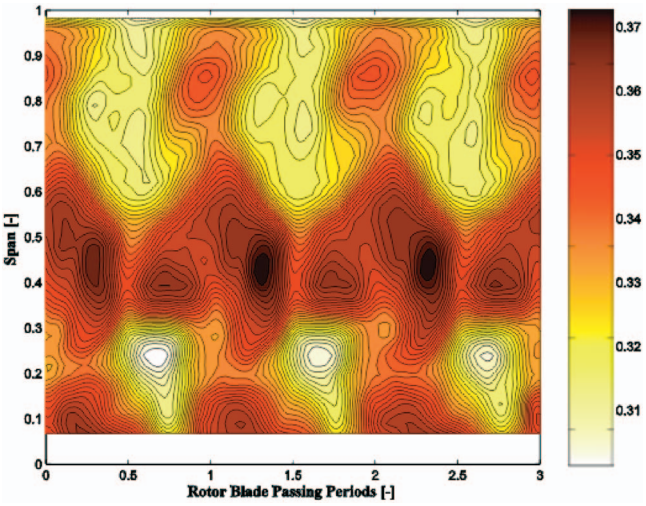

Fig. 19 Circumferentially mass-averaged distribution of measured total pressure coefficients at exit of stator 2, plotted versus time of three rotor blade passing periods

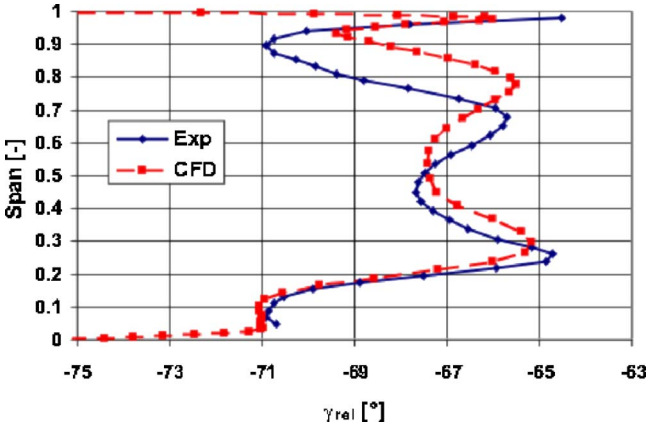

Fig. 21 Comparison of relative exit flow angle behind the rotor between time-averaged experimental results and CFD

pitches shown, the variation of total pressure between the two appears to be significant. Depending on how much secondary flow of the rotor is arriving at the stator exit the total pressure in the stator passage exit changes considerably. The change of total pressure over time would have an effect on the loading of a downstream rotor. In order to visualize the effective impact on a following blade row, Figs. 19 and 20 show the time-resolved evolution of circumferentially mass-averaged total pressure coefficient and absolute flow yaw angle. Since both plots show the exit flow field of a stationary blade row, any variation over time is due to secondary flows of the upstream rotor interacting with the stationary flow field of the stator. In Fig. 19 from 60% to 100% the *Cpt* values are reduced for about half of the time of a rotor blade passing period. This reduction originates from the interaction of the rotor tip passage vortex and tip leakage vortex with the secondary flow of the stator. An analogu behavior can be seen from 20% to 30% span, which relates to the rotor hub passage vortex.

In terms of flow angles the interaction of secondary flows creates a variation of circumferentially mass-averaged yaw angles over time of around ±2.5 deg (see Fig. 21). Hereby the maxima and minima are timewise shifted relative to each other. The inlet flow into a consecutive rotor would receive some incidence from the stator. However, the influence of the unsteady static pressure field of this rotor has to be taken into account as well in order to make a definite statement on the unsteady flow angle distribution.

Comparison of Numerical and Experimental Results. The evaluation of the experimental data has shown differences in the measured flow field with respect to the CFD prediction. In order to reduce the computational time, the calculations for the design of the turbine were done with a relatively coarse grid comprising 60 cells in a radial direction. Pressure levels inbetween the blade rows could be predicted very well. However, positions of secondary flow features, such as vortices, have shown larger deviations from the numerical prediction. In Fig. 21 the spanwise distributions of relative rotor exit flow angles from CFD and time-averaged experimental results are presented. The extension from the casing of the over–under turning region of the tip leakage and tip passage vortex is underpredicted by the CFD by about 10% span. An improvement of the CFD results could possibly be achieved by applying an improved grid definition, which is capable of resolving the complex flow features responsible for the tip leakage flow phenomena.

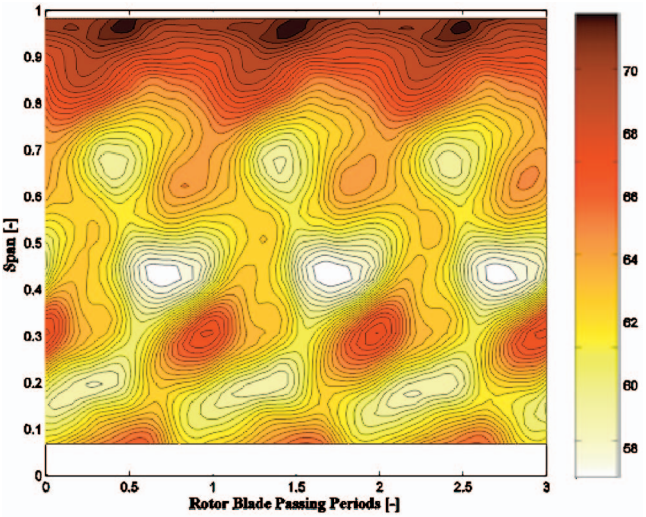

Fig. 20 Circumferentially mass-averaged distribution of measured absolute flow yaw angle at exit of stator 2, plotted versus time of three rotor blade passing periods

Conclusions

A new 1 1/2-stage, unshrouded research turbine test case has been designed and built within the Turbomachinery Laboratory of ETH Zurich in order study novel methods of reducing rotor tip leakage losses. The new turbine case has been extensively tested applying unsteady and steady probe measurement techniques. The results were analyzed with particular attention on the flow region at the rotor tip gap and the flow interactions between the different bladerows.

The geometry of the 1 1/2-stage turbine models a highly loaded, low aspect ratio gas turbine environment. The measured performance of the first stage reflects very well the design intent: loading coefficient of 2.36 and flow coefficient of 0.65 at a total pressure ratio of 1.35 and a degree of reaction of 0.39. Stator exit Mach numbers of up to Ma=0.58 ensure a realistic flow environment, which shows compressibility effects, but still allows the application of intrusive unsteady measurement techniques. Probe measurement access is provided at various locations around all bladerows. In addition a multi-purpose window inside the rotor casing covering a circumferential distance of five rotor pitches gives optical access to the inside of the rotor bladerow.

The results of the probe measurements represent a rare set of data, which describes the unsteady flow in a 1 1/2-stage turbine.

The geometry and flow field data of the turbine will be available to the turbomachinery community for validation and improvement of numerical tools.

The secondary flow features of the first stator are almost perfectly radially aligned. This implies that stator wake and passage vortices affect the rotor blade almost simultaneously. This is also the reason for a pulsation of total pressure in the rotor inlet flow field, modulated by the rotor leading edge.

The pulsation of the rotor inlet flow field manifests itself as well in the rotor inlet flow angles. Circumferentially mass-averaged flow yaw angles vary by ±2.5 deg during the time of one blade passing period. In the rotor tip region temporary negative incidence of 40 deg could be seen due to these blade row interactions. This phenomenon will introduce increased unsteadiness into the development of the rotor tip leakage flow.

Remnants of the first stator secondary flows have been found to affect the location of secondary flow features of the rotor. The rotor hub passage vortex shows a temporary radial inward migration of 10% blade span during the time of one blade passing period.

At the exit of the second stator the circumferentially mass-averaged flow yaw angles vary by ±2.5 deg. In this case this variation can only be attributed to the interaction between the rotor and the second stator, since no further bladerow is following downstream. The unsteadiness introduced upstream of the second stator propagates through the blade row and causes this high angle fluctuation.

The vortices of the rotor get modulated by the leading edges of the second stator. A variation of vortex size and relative position to the rotor trailing edge has been detected. Due to the 2:3 ratio of blade count between rotor and stators the interaction of the trailing edges of two neighboring rotor blades with the leading edges of the second stator is time shifted. This leads to a varying circumferential distance between the vortices of two neighboring rotor blades due to their deflection around the second stator leading edges. The variation in distance has been determined for the tip leakage vortices to be on the order of ±20% of a rotor pitch.

Nomenclature

c = absolute flow velocity (m/s)
c_p = specific heat capacity at constant pressure (J/kg K)
Cps = static pressure coefficient, $Cps=p-p_3/p_{t0}-p_3$ (-)
Cpt = total pressure coefficient, $Cpt=(p_t-p_3)/(p_{t0}-p_3)$ (-)
h = enthalphy (kJ/kg)
$\dot{m}$ = massflow (kg/s)
M = torque (N m)
p = pressure (Pa)
R = perfect gas constant (J/kg K]
r = radius (m)
T = temperature (K)
u = rotational speed (m/s)

Greek Symbols

ε = turning angle (deg)
ψ = loading coefficient ($\psi=\Delta h/u^2$) (-)
ϕ = flow coefficient $\phi=c_x/u$ (-)
ϕ = flow yaw angle (positive in rotor turning direction) (deg)
γ = flow pitch angle (positive towards casing) (°)
κ = isentropic coefficient ($\kappa=c_p/c_v$) (−)
ω = rotational velocity (1/s)

Abbreviations

5HP = five-hole probe
CFD = computational fluid dynamics
CoG = center of gravity
FRAP = fast response aerodynamic probe
LE = leading edge
MP = measurement plane
TE = trailing edge
TET = turbine entry temperature

Subscripts

av = average
m = mechanical
rel = relative frame of reference
t = total
th = thermal
x = axial direction

References

[1] Booth, T. C., 1982, "Rotor-Tip Leakage Part I—Basic Methodology," J. Eng. Power, **104**, pp. 154–161.
[2] Denton, J. D., 1993, "Loss Mechanisms in Turbomachines," ASME J. Turbomach., **115**, pp. 621–656.
[3] Booth, T. C., 1985, "Importance of Tip Leakage Flows in Turbine Design," VKI Lecture Series 1985-05, "*Tip Clearance Effects in Axial Turbomachines*," 1985.
[4] Bindon, J. P., and Morphis, G., 1990, "The Development of Axial Turbine Leakage Loss for Two Profiled Tip Geometries Using Linear Cascade Data," ASME Paper No. 90-GT-152, June.
[5] Kaiser, I., and Bindon, J. P., 1997, "The Effect of Tip Clearance on the Development of Loss Behind a Rotor and a Subsequent Nozzle," ASME Paper No. 97-GT-53.
[6] Yoshino, S., 2002, "Heat Transfer in Rotating Turbine Experiments," Ph.D. thesis, Oxford University, Oxford, UK.
[7] Camci, C., Dey, D., and Kavurmacioglu, L., 2003, "Tip Leakage Flows in Near Partial Squealer Rims in an Axial Flow Turbine Stage," ASME Paper No. GT2003-38979.
[8] Chander, P., Lee, C.-P., Cherry, D., Wadia, A., and Doughty, R., 2005, "Analysis of Some Improved Blade Tip Concepts," ASME Paper No. GT2005-68333.
[9] De Cecco, S., Yaras, M. I., and Sjolander, S. A., 1995, "Measurement of Tip Leakage Flows in Turbine Cascade with Large Clearances," ASME Paper No. 95-GT-77.
[10] Yamamoto, A., Tominaga, J., Matsunuma, T., and Outa, E., 1994, "Detailed Measurements of Three-Dimensional Flows and Losses Inside an Axial Flow Turbine Rotor," ASME Paper No. 94-GT-348.
[11] Staubach, J. B., Sharma, O. P., and Stetson, G. M., 1996, "Reduction of Tip Clearance Losses Through 3-D Airfoil Designs," ASME Paper No. 96-TA-13.
[12] Offenburg, L. S., Fischer, J. D., and Hoek, T. J. V., 1987, "An Experimental Investigation of Turbine Case Treatments," AIAA-87-1919.
[13] Harvey, N. W., 2004, "Aerothermal Implications of Shroudless and Shrouded Blades," VKI Lectures Series 2004-02, "*Turbine Blade Tip Design and Tip Clearance Treatment*."
[14] Dey, D., and Camci, C., 2000, "Development of Tip Clearance Flow Downstream of a Rotor Blade With Coolant Injection From a Tip Trench," *Proceedings of the 8th ISROMAC Conference*, Honolulu, Hawaii, pp. 572–579.
[15] Rao, N. M., and Camci, C., 2004, "Axial Turbine Tip Desensitization by Injection from a Tip Trench, Part 1: Effect of Injection Mass Flow Rate," ASME Paper No. GT2004-53256.
[16] Rao, N. M., and Camci, C., 2004, "Axial Turbine Tip Desensitization by Injection from a Tip Trench, Part 2: Leakage Flow Sensitivity to Injection Location," ASME Paper No. GT2004-53258.
[17] Schlienger, J., 2003, "Evolution of Unsteady Flows in a Multistage Shrouded Axial Turbine," Ph.D. dissertation No. 15230, ETH, Zurich, Switzerland.
[18] Pfau, A., 2003, "Loss Mechanisms in Labyrinth Seals of Shrouded Axial Turbines," Ph.D. dissertation No. 15226, ETH, Zurich, Switzerland.
[19] Porreca, L., Behr, T., Schlienger, J., Kalfas, A. I., and Abhari, R. S., 2005, "Fluid Dynamics and Performance of Partially and Fully Shrouded Axial Turbines," ASME J. Turbomach., **127**, pp. 668–678.
[20] Behr, T., Porreca, L., Mokulys, T., Kalfas, A. I., and Abhari, R. S., 2006, "Multistage Aspects and Unsteady Flow Effects of Stator and Rotor Clocking in an Axial Turbine with Low Aspect Ratio Blading," ASME J. Turbomach., **128**, pp. 11–22.
[21] Sell, M., Schlienger, J., Pfau, A., Treiber, M., and Abhari, R. S., 2001, "The 2-Stage Axial Turbine Test Facility LISA," ASME Paper No. 2001-GT-0492.
[22] Behr, T., Kalfas, A. I., and Abhari, R. S., 2006, "Geometry Data of Unshrouded 1.5-Stage Turbine Profiles," http://www.lsm.ethz.ch
[23] Pritchard, L. J., 1985, "An Eleven Parameter Axial Turbine Airfoil Geometry Model," ASME Paper No. 85-GT-219.
[24] Troxler, A., 2002, "Inverse Design of Gas Turbine Components," *Proceedings 4th International Conference on Inverse Problems in Engineering*, Rio de Janeiro, Brazil.
[25] Dawes, W. N., 1988, "Development of a 3-D Navier-Stokes Solver for Application to All Types of Turbomachinery," ASME Paper No. 88-GT-70.
[26] Jameson, A., and Baker, T. J., 1984, "Multigrid Solutions of the Euler Equations for Aircraft Configurations," AIAA Paper No. 84-0093.
[27] Spalart, P. R., and Allmaras, S. R., 1992, "A One-Equation Turbulence Model for Aerodynamic Flows," AIAA Report No. 92–0439.

[28] Mokulys, T., Dewhurst, S., and Abhari, R. S., 2005, "Numerical Validation of Characteristics and Linearized Unsteady Boundary Conditions for Non-Integer Blade Ratios in a Non-Linear Navier–Stokes Solver," ASME Paper No. GT2005-68670.
[29] Kupferschmied, P., Köppel, O., Gizzi, W. P., and Gyarmathy, G., 2000, "Time Resolved Flow Measurements With Fast Aerodynamic Probes in Turbomachinery," Meas. Sci. Technol., **11**, pp. 1036–1054.
[30] Pfau, A., Schlienger, J., Kalfas, A. I., and Abhari, R. S., 2002, "Virtual Four Sensor Fast Response Aerodynamic Probe (FRAP)," *Proceedings of the 16th Bi-Annual Symposium on Measuring Techniques in Transonic and Supersonic Flows in Cascades and Turbomachines*, Cambridge, UK, Sept. 23–24.
[31] Porreca, L., Hollenstein, M., Kalfas, A. I., and Abhari, R. S., 2007, "Turbulence Measurements and Analysis in a Multistage Axial Turbine," J. Propul. Power, **23**, pp. 227–234.
[32] Smith, S. F., 1963, "A Simple Correlation of Turbine Efficiency," J. R. Aeronaut. Soc., **69**, pp. 467–470.
[33] Chaluvadi, V. S. P., Kalfas, A. I., Hodson, H. P., Ohyama, H., and Watanabe, E., 2003, "Blade Row Interaction in a High-Pressure Steam Turbine," ASME J. Turbomach., **125**, pp. 14–24.